Investigating [redacted] the Interleaving QSW VRM

Pit-Leong Wong, Qiaoqiao Wu, Peng Xu, Bo Yang and Fred C. Lee

Center for Power Electronics Systems
The Bradley Department of Electrical and Computer Engineering
Virginia Polytechnic Institute and State University
Blacksburg, VA 24061 USA

Abstract – **The multi-channel interleaving quasi-square-wave (QSW) buck converter has been proved to be suitable for the voltage regulator module (VRM) with low voltage, high current and fast transient response. Integrated magnetic is used to reduce the size of the converter and improve efficiency. However, the structure of the integrated magnetic requires precise adjustment. In this paper, analysis shows that a properly designed integrated magnetic can improve the steady-state and dynamic performance without requiring precise adjustment.**

I. INTRODUCTION

Processors of future computers are expected to demand low voltage about 1V and consume higher current with higher clock rate. The increasing steady-state and dynamic requirements impose challenges to the design of the voltage regulator module (VRM) in future computer power systems.

The multi-channel interleaving quasi-square-wave (QSW) proposed by CPES/VPEC is a very promising structure as far as meeting these future VRM specifications [2-4], and has been widely adopted as industry practice. For simplicity, only two-channel interleaving (Figure 1) is considered in this paper.

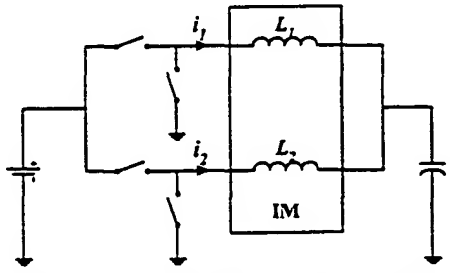

Figure 1 Interleaving quasi-square-wave converter

The multi-channel interleaving structure requires more inductors, which increases the complexity of the circuit. To reduce component counts, integrated magnetics can be used to build the two individual inductors of the two interleaving channels on a single pair of EE or EI cores [1]. The two inductors are in the shaded area in Figure 1. The structure of the integrated inductor is shown in Figure 2. The two inductors are built on the two outer legs of the core. An air gap is required on each outer leg to avoid saturation of the core. To provide a low magnetic reluctance path for the flux generated by the two windings so that the two inductors can be decoupled, no air gap is used on the center leg. The sum of the two fluxes generated by the two windings goes through the center leg. Due to the phase shift in the interleaving structure, the AC magnetic flux ripple in the center leg can be reduced, which reduces the core loss of the center leg, and improves the overall efficiency.

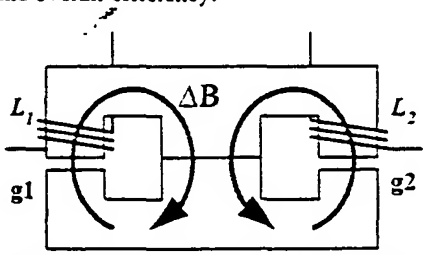

Figure 2 Core structure of the integrated magnetic

However, this kind of magnetic core is not a standard industry practice. The core requires high precision adjustment. The two pieces of the core only connect to each other at the center leg. To ensure mechanical stability, gap filling must be used in the air gaps of the two outer legs. Because no air gap is allowed in the center leg, the thickness of the two outer leg gaps must be filled exactly. This precision makes mass production difficult and costly. Moreover, because the air gap cannot be adjusted to achieve different inductance as it is in conventional inductor design, once the core is cut, only one inductance value can be obtained. This restriction also reduces the flexibility of the core.

This paper investigates the implementation of integrated inductors using core structures that do not require very precise technology.

II. EFFECT OF THE COUPLING INDUCTOR ON CONVERTER PERFORMANCE

The core structure for the integrated inductor under analysis is shown in Figure 3. The difference between this structure and the structure in Figure2 is the air gap in the center leg. Since there is an air gap in the center leg of this structure, the outer leg air gap fillings do not need to be so exact.

APEC' 2000

0-7803-5867-8/00/$10.00 (c) 2000 IEEE

Because of the air gap, the center leg is no longer a low magnetic reluctance path for the fluxes. The flux generated by the winding of L_1 can go through all three legs if the winding of L_2 is open-circuit. The flux generated by the winding of L_2 has a similar path. The flux interaction between the windings (the dotted line in Figure 3) indicates the coupling effect these two inductors have on each other.

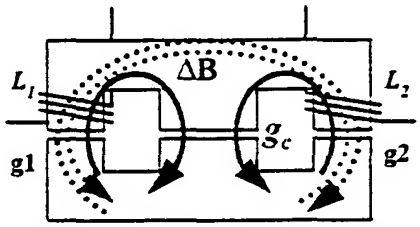

Figure 3 Core structure of the proposed integrated magnetic

The two inductors built on this structure cannot be considered as two individual inductors as it is in Figure 1. The two output inductors have a coupling inductance M as shown in Figure 4.

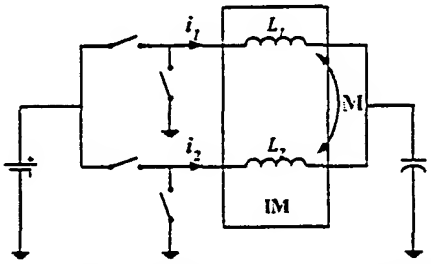

Figure 4 Interleaving converter with coupling output inductor

The two inductors can be directly coupled or inversely coupled because of the different directions of the two windings. There are two identical equivalent circuits for each coupling format (Figure 5).

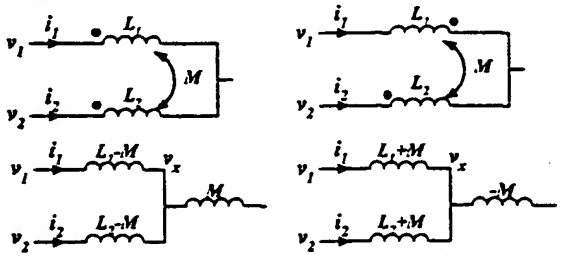

(a) direct coupling (b) inverse coupling

Figure 5 Two different patterns of the coupling inductor

For direct coupling, the circuit can be described by two identical sets of formulas:

$$\begin{cases} v_1 = L_1 \cdot \dfrac{di_1}{dt} + M \cdot \dfrac{di_2}{dt} \\ v_2 = M \cdot \dfrac{di_1}{dt} + L_2 \cdot \dfrac{di_2}{dt} \end{cases} \quad (1)$$

and

$$\begin{cases} v_1 - v_x = (L_1 - M) \cdot \dfrac{di_1}{dt} \\ v_2 - v_x = (L_2 - M) \cdot \dfrac{di_2}{dt} \\ v_x = M \cdot \dfrac{d(i_1 + i_2)}{dt} \end{cases} \quad (2)$$

For inverse coupling, the corresponding formulas are:

$$\begin{cases} v_1 = L_1 \cdot \dfrac{di_1}{dt} - M \cdot \dfrac{di_2}{dt} \\ v_2 = -M \cdot \dfrac{di_1}{dt} + L_2 \cdot \dfrac{di_2}{dt} \end{cases} \quad (3)$$

and

$$\begin{cases} v_1 - v_x = (L_1 + M) \cdot \dfrac{di_1}{dt} \\ v_2 - v_x = (L_2 + M) \cdot \dfrac{di_2}{dt} \\ v_x = -M \cdot \dfrac{d(i_1 + i_2)}{dt} \end{cases} \quad (4)$$

where v_1 and v_2 are the voltages applied on the two corresponding windings. There are two possible voltage values for v_1 and v_2: v_a corresponds to the turn-on of the top switches; and v_b corresponds to the turn-on of the bottom switches.

$$v_a = V_{in} - V_O \quad (5)$$

$$v_b = -V_O \quad (6)$$

The waveforms for v_1 and v_2 are shown in Figure 6. Considering the different cases of duty cycle D<0.5 and D>0.5, there are four different cases in all.

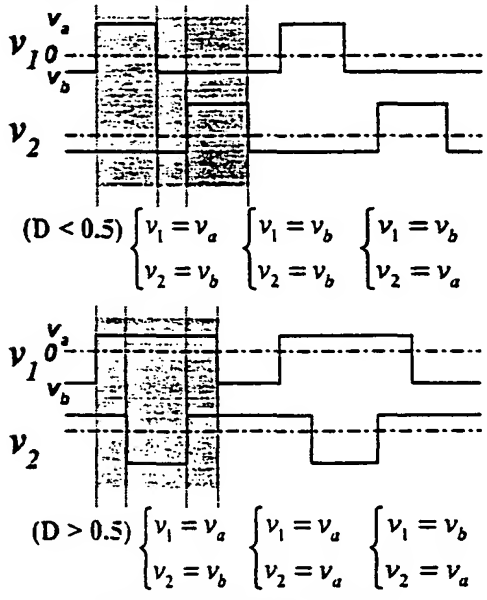

Figure 6 Inductor voltage waveforms

0-7803-5867-8/00/$10.00 (c) 2000 IEEE

Because the voltage-second of the inductors balances for each cycle during steady state, there exists $D \cdot v_a = D' \cdot v_b$. The equivalent inductors for each case are shown in the following formulas.

$$\begin{cases} v_1 = v_a \\ v_2 = v_b \end{cases} \Rightarrow v_1 = \frac{L^2 - M^2}{L + \frac{D}{D'} \cdot M} \cdot \frac{di_1}{dt} \qquad L_{eq} = \frac{L^2 - M^2}{L + \frac{D}{D'} \cdot M}$$

$$\begin{cases} v_1 = v_b \\ v_2 = v_b \end{cases} \Rightarrow v_1 = (L + M) \cdot \frac{di_1}{dt} \qquad L_{eq} = L + M$$

$$\begin{cases} v_1 = v_a \\ v_2 = v_a \end{cases} \Rightarrow v_1 = (L + M) \cdot \frac{di_1}{dt} \qquad L_{eq} = L + M$$

$$\begin{cases} v_1 = v_b \\ v_2 = v_a \end{cases} \Rightarrow v_1 = \frac{L^2 - M^2}{L + \frac{D}{D'} \cdot M} \cdot \frac{di_1}{dt} \qquad L_{eq} = \frac{L^2 - M^2}{L + \frac{D}{D'} \cdot M} \qquad (7)$$

There are only two different equivalent inductors for all the cases: ***Leq1*** for $v_1 = v_2$, and ***Leq2*** for $v_1 \neq v_2$. Because of the phase shift of the interleaving channels, different voltages are applied to the two windings for most of time during steady state. During converter transient response, the two windings have the same voltage when the duty cycle ratio is close to saturation. Approximately, ***Leq1*** can be considered as the inductor during the transient response, and ***Leq2*** as the inductor for steady state. A larger inductance corresponds to a smaller steady-state current ripple, which has a smaller root-mean-square (RMS) value and causes smaller conduction loss in the MOSFET and other components in the circuit. Smaller inductance corresponds to a faster transient response. From the performance viewpoint, small ***Leq1*** and large ***Leq2*** are preferred.

In direct coupling, there exists M>0. Thus,

$$\begin{cases} L_{eq1} = L + M > L \\ L_{eq2} = \frac{L^2 - M^2}{L + \frac{D}{D'} \cdot M} < L \end{cases}, \qquad (8)$$

This will worsen the performance. The steady-state current waveforms for the two inductors are shown in Figure 7(a). The dotted line is the current waveform for the interleaving converter without coupling inductors. Direct coupling results in larger steady-state current ripples for both the cases of D>0.5 and D<0.5.

In inverse coupling, there exists M<0. Thus,

$$\begin{cases} L_{eq1} = L + M < L \\ L_{eq2} = \frac{L^2 - M^2}{L + \frac{D}{D'} \cdot M} > L \end{cases}, \qquad (9)$$

if

$$|M| < \min\left(\frac{D}{D'}L, \frac{D'}{D}L\right). \qquad (10)$$

This indicates that, for proper inverse coupling between the two windings, the steady state current ripple of the converter can be reduced without slowing down the transient response. Figure 7(b) shows the steady state inductor current waveforms when Formula (10) is satisfied. For both the cases of D>0.5 and D<0.5, the current ripple is smaller than that for non-coupling inductors.

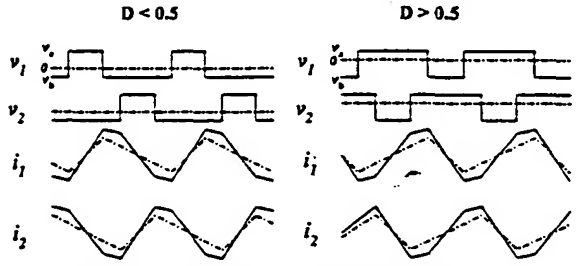

(a) Inductor current for direct coupling output inductors

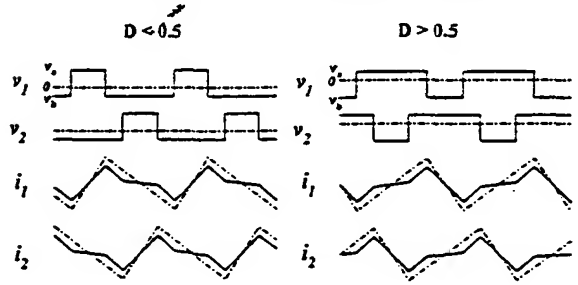

(b) Inductor current for inverse coupling output inductors

Figure 7 Steady-state current waveforms for coupling output inductors

III. DESIGN AND SIMULATION RESULTS

The previous section shows the possibility of performance improvement by the use of coupling inductors. The design issues of the core will be discussed in this section. Figure 8 shows the relationship between the coupling effect (***M/L***) and the normalized steady state equivalent inductance (***Leq2/L***). The design should be in the region of ***Leq2>L***, where the steady state conduction loss can be reduced. The region shrinks as the duty cycle ratio decreases.

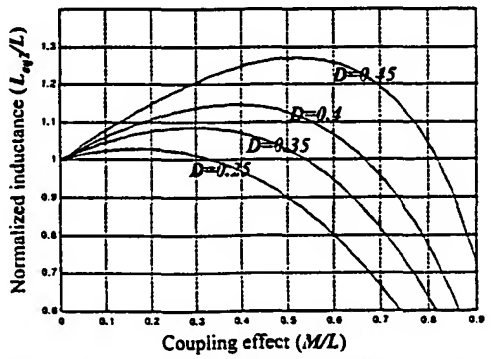

Figure 8 Normalized equivalent inductance of different coupling effects

0-7803-5867-8/00/$10.00 (c) 2000 IEEE

Figure 9 shows the magnetic analog circuit for the core structure shown in Figure 3. The magnetic reluctance of the three legs, R_1, R_2 and R_c, can be determined by the following formula:

$$R_i = \sum_k \frac{l_k}{\mu_k \cdot A_k} \qquad (i = 1, 2, c). \tag{11}$$

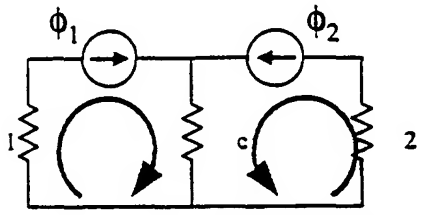

Figure 9 Magnetic analog circuit of the core

The flux, ϕ_1 and ϕ_2, is only determined by the voltage-second of the corresponding winding.

$$\begin{cases} \phi_1 = \int \frac{v_1}{N_1} dt \\ \phi_2 = \int \frac{v_2}{N_2} dt \end{cases} \tag{12}$$

Based on the Ampere's Law and the continuity of flux, for each loop in Figure 9, there exists:

$$\sum \phi \cdot R = N_i \cdot i_i \tag{13}$$

$$\begin{cases} R_1 \cdot \phi_1 + R_c \cdot (\phi_1 + \phi_2) = N_1 \cdot i_1 \\ R_2 \cdot \phi_2 + R_c \cdot (\phi_1 + \phi_2) = N_2 \cdot i_2 \end{cases} \tag{14}$$

The flux of each leg can then be found:

$$\begin{cases} \phi_1 = \frac{N_1 \cdot (R_2 + R_c)}{\Delta} \cdot i_1 - \frac{N_2 \cdot R_c}{\Delta} \cdot i_2 \\ \phi_2 = -\frac{N_1 \cdot R_c}{\Delta} \cdot i_1 + \frac{N_2 \cdot (R_1 + R_c)}{\Delta} \cdot i_2 \end{cases}, \tag{15}$$

where

$$\Delta = R_1 \cdot R_2 + R_1 \cdot R_c + R_2 \cdot R_c . \tag{16}$$

The differential of Formula (15) is:

$$\begin{cases} v_1 = N_1 \cdot \frac{d\phi_1}{dt} = \frac{N_1^2 \cdot (R_2 + R_c)}{\Delta} \cdot \frac{di_1}{dt} - \frac{N_1 \cdot N_2 \cdot R_c}{\Delta} \cdot \frac{di_2}{dt} \\ v_2 = N_2 \cdot \frac{d\phi_2}{dt} = -\frac{N_1 \cdot N_2 \cdot R_c}{\Delta} \cdot \frac{di_1}{dt} + \frac{N_2^2 \cdot (R_1 + R_c)}{\Delta} \cdot \frac{di_2}{dt} \end{cases} \tag{17}$$

The inductance and the coupling effect between the two windings can be found by comparing Formula (17) with Formula (3).

$$\begin{cases} L_1 = \frac{N_1^2 \cdot (R_2 + R_c)}{\Delta} \\ L_2 = \frac{N_2^2 \cdot (R_1 + R_c)}{\Delta} \\ M = \frac{N_1 \cdot N_2 \cdot R_c}{\Delta} \end{cases} \tag{18}$$

For simplification, let $N_1 = N_2$ and

$$\begin{cases} R_1 = R_2 = \frac{g_1}{\mu_o \cdot A_1} \\ R_c = \frac{g_c}{\mu_o \cdot A_c} \end{cases} \tag{19}$$

Then,

$$\frac{M}{L} = \frac{R_c}{R_1 + R_c} = \frac{g_c}{\frac{A_c}{A_1} \cdot g_1 + g_c} . \tag{20}$$

The magnetic core can be designed to achieve *Leq2>L*, based on Formula (20) and Figure 8. A design structure with a commercial E-I core of $A_c = 2 \cdot A_1$ and the same air gap for all three legs (which is the easiest application of the core) will be used for the remaining analyses and simulations. From Formula (20), *M/L* = 1/3. For converter input voltage Vin = 5V, and output voltage Vo=2V, the duty cycle ratio D = 0.4. From Figure 8, L_{eq}/L = 1.15. The current waveforms in the two coupling inductors have smaller ripples compared to those in non-coupling inductors, which have a peak-to-peak value of 13A (Figure 10).

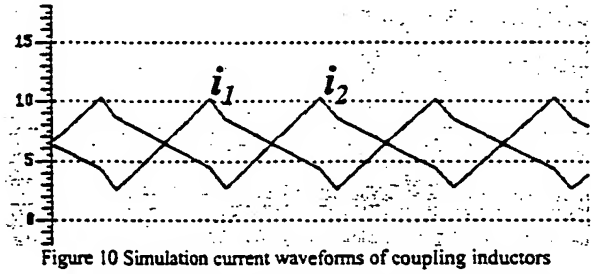

Figure 10 Simulation current waveforms of coupling inductors

Figure 11 shows the magnetic flux waveform in the core, which is the same as that in the non-coupling core. The flux in the two outer legs, *ϕ1* and *ϕ2*, is determined by the voltage-second applied to the corresponding windings. The flux in the center leg, which is the sum of the flux in the outer legs, has a much smaller ripple. Thus, the core loss in the center leg can be reduced. The flux ripple cancellation effect is the same as that in the non-coupling core, which can be more easily understood from Figure 9. The difference between the non-coupling and inverse coupling integrated inductors is that the magnetic reluctance in the center leg is zero in a non-coupling situation. No matter what the reluctance is, the flux

0-7803-5867-8/00/$10.00 (c) 2000 IEEE

is always the sum of $\phi 1$ and $\phi 2$ in the center leg. The flux waveforms remain unchanged as long as the voltage-second and the turn number of the windings stay the same.

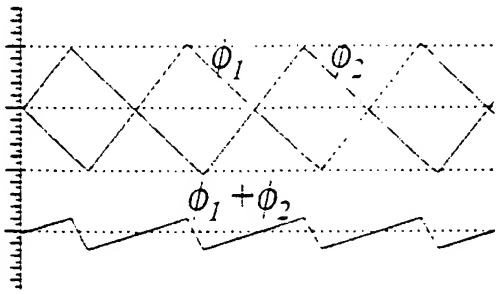

Figure 11 Flux waveforms of the core

The previous analysis is based on the average flux viewpoint. The result can be different in finite element analysis. Figure 12 shows the finite element analysis results of the AC magnetic flux distribution in the cores for different integrated inductor structures. A sinusoidal current waveform at the switching frequency is used in the simulation. The magnitude of the sinusoidal waveform is the peak-to-peak value of the inductor current. The red areas correspond to high AC flux magnitude, while the blue areas correspond to low AC flux magnitude.

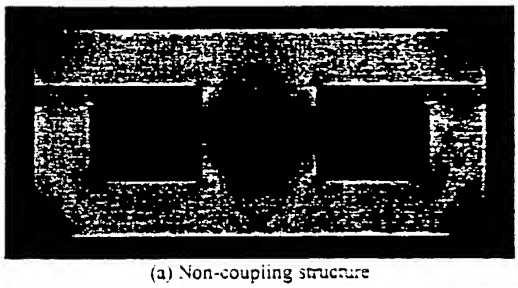

(a) Non-coupling structure

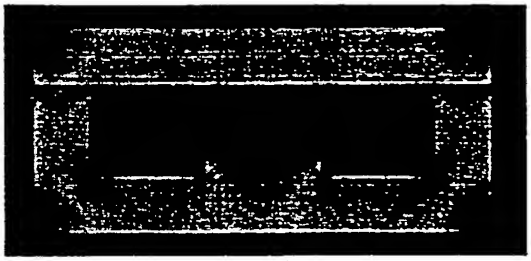

(b) Inverse coupling structure

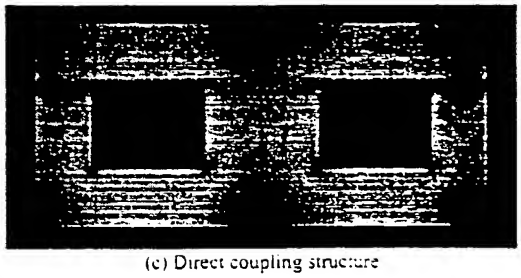

(c) Direct coupling structure

Figure 12 Flux distribution in the core

In a non-coupling structure, although the average AC flux is zero in the center leg, there are still flux-crowded areas. The low magnetic impedance in the center leg causes this uneven flux distribution. The AC flux-crowded areas generate large core losses, which are the hot spots in the core. In the inverse coupling structure, the air gap in the center leg increases the magnetic impedance, which makes the flux more evenly distributed in the center leg (Figure 12). The inverse coupling structure is expected to have smaller magnetic core loss in the center leg than the non-coupling structure because of this even flux distribution.

For direct coupling, the flux in the center leg is the difference between $\phi 1$ and $\phi 2$ ($\phi_C = \phi_1 - \phi_2$). The AC flux magnitude is the sum of $\phi 1$ and $\phi 2$. The magnetic core loss in the center leg is similar to that in the two outer legs. From the standpoint of core loss, there is no benefit for this inductor integration structure.

The preceding analysis shows that properly designed integrated output inductors with inverse coupling can improve steady-state efficiency.

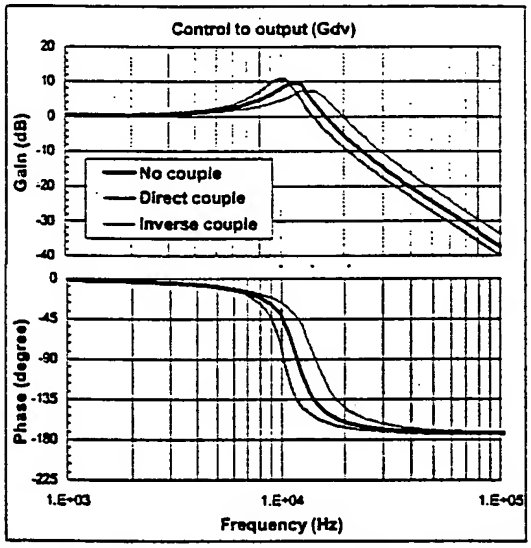

Figure 13 Small signal models of two-channel interleaving buck

Figure 13 gives the simulation results of the control-to-output transfer functions for the two-channel interleaving buck converters shown in Figures 1 and 4. The small signal model is similar to a single-channel buck converter. The only difference is the effective inductance, which determines the double poles of the model. For non-coupling output inductors, the effective inductance is:

$$L_{eff} = \frac{L}{2}, \tag{20}$$

where L is the inductance of each channel. For coupling output inductors, the effective inductance is:

$$L_{effC} = \frac{L-M}{2} + M. \tag{21}$$

0-7803-5867-8/00/$10.00 (c) 2000 IEEE

The coupling inductance M is positive in direct coupling and negative in inverse coupling. In inverse coupling, $L_{effC} < L_{eff}$, while for direct coupling, $L_{effC} > L_{eff}$. The different effective output inductance can be obviously seen from the transfer functions in Figure 13.

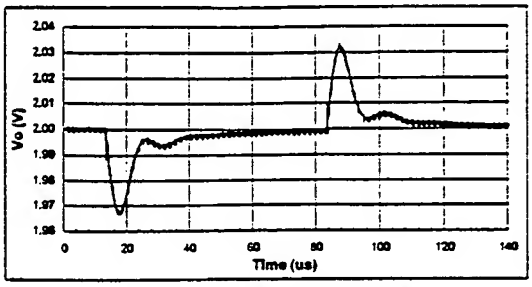

(a) Non-coupling output inductors

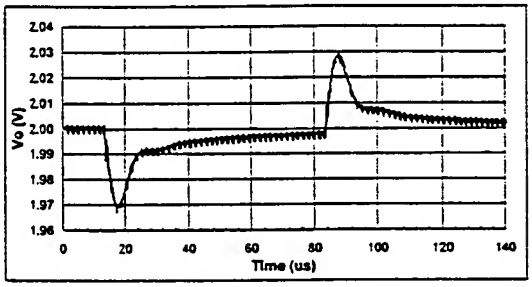

(b) Inverse coupling output inductors

Figure 14 Output voltage transient waveforms.

Figure 14 gives the simulation result of transient voltage waveforms at the VRM output. The inductance in the two cases is 300nH for each channel. The current step is 13A. The bandwidth of the feedback control stays the same (about 100kHz) in both cases. The transient response is similar in both the non-coupling and inverse coupling output inductors.

IV. CONCLUSION

This paper analyzes the effect of the integrated coupling inductor on the interleaving buck converters. It shows that with proper design the inverse coupling integrated inductors can improve the steady state efficiency of the converter, while maintaining the fast dynamic response. Inverse coupling output inductors cause smaller steady-state current ripples, which can reduce the RMS-related conduction losses in the circuit. AC magnetic flux ripple cancellation can be achieved in the center leg of the integrated structure. The air gap in the center leg makes the flux more evenly distributed, which can reduce the core loss in the center leg. Less precise manufacturing requirements should reduce the cost of mass producing this structure.

REFERENCE

[1] W. Chen and F. C. Lee, "Integrated Inductor Scheme for Multi-Module Interleaved Quasi-Square-Wave DC/DC Converter," APEC 1999.

[2] X. Zhou, P. Wong, R. Watson, L. Amoroso, X. Sun, H. Wu, P. Xu, B. Yang, F. C. Lee and A. Q. Huang, "Investigation of Power Management Issues for Next Generation Intel Microprocessors: Quarterly Progress Report," VPEC, 1998.

[3] P. Wong, X. Zhou, J. Chen, H. Wu, L. Amoroso, J. Liu, F. C. Lee, X. Zhang and D. Y. Chen, "VRM Transience Study and Output Filter Design for Future Processors," VPEC Seminar 1997.

[4] X. Zhou, J. Liu, X. Zhang, P. Wong, J. Chen, H. Wu, L. Amoroso, F. C. Lee, and D. Y. Chen, "Investigation of Candidate VRM Topology for Future Microprocessors," VPEC Seminar 1997.

[5] W. Chen, G. Hua, D. Sable and F. C. Lee, "Design of High Efficiency, Low Profile Low Voltage Converter with Integrated Magnetics," VPEC Seminar 1997.

[6] S. Goodfellow and D. Weiss, "Design Power Systems Around Processor Specifications," Electronic Design, January 1997.

[7] M. Zhang, M. Jovanovic and F. C. Lee, "Design Considerations for Low-Voltage On-board DC/DC Modules for Next Generations of Data Processing Circuits," IEEE Transactions on Power Electronics, Vol. 11, No. 2, March 1996.

0-7803-5867-8/00/$10.00 (c) 2000 IEEE